

Thermo-Viscoplastic Material Modelling for Self-heating Loads and its Experimental Verification

Holger Sparr*, Robert Roszak, Ilja Sagradov, Daniela Schob and Matthias Ziegenhorn

BTU Cottbus–Senftenberg, Universitätsplatz 1, 01968 Senftenberg, Germany

Abstract: The paper examines a modelling approach for thermomechanically coupled problems and an experimental concept for a material law validation and verification for self-heating with small to moderate temperature ranges. The study compares two different model formulations and is generally applicable to a variety of material classes. One model is based on a rheological network with an extension for dissipative deformation below the elastic limit. The other model operates without a yield condition. Both models are applied to published experimental data in terms of rate-independent behaviour and the evaluation is carried out on stress-strain-level, temperature evolution and the energy transformation ratio. Furthermore the two models are applied to a strain rate-dependent load case conducted at our institute discussing the same entities. It is pointed out, that the approach of a thermomechanical analysis is valuable and informative to assess the observed deformation processes and to describe the material behaviour with a thermodynamically valid parameter set.

Keywords: Thermomechanics, self-heating, viscoplasticity, energy transformation ratio, thermography

1 Introduction

The foundation of the thermomechanical analysis was given by THOMSON's work and the publication of the thermoelastic effect Thomson (1853). By the end of the 1960ies, the fully coupled thermomechanical problem was formulated in the framework of continuum mechanics enhanced with the concept of internal state variables (see Truesdell and Noll (2004); Coleman and Gurtin (1967)).

In the same period, scientists exploited the often experimentally observed temperature build-up during cyclic mechanical testing. OLDYREV and others tried to quantify fatigue properties related to damage in glass fibre reinforced plastics by measuring the temperature evolution by thermocouples (see Oldyrev (1967); Oldyrev and Tamuzh (1969)).

Since then, the experimental equipment has improved towards contact-free measurement principles, which has led to high-resolution infrared (IR) camera systems. This development initialised a new series of publications dealing with thermomechanics from the theoretical and/or experimental point of view. The general principle of IR cameras is limited to certain temperature ranges but not restricted to any specific material class, since thin black coatings improve reflection and radiation properties and do not effect the thermomechanical properties of the specimen [Ummenhofer and Medgenberg (2006); Chrysochoos (2012); Fedorova et al. (2014); Cholewa et al. (2016)].

In general, a deformation process can be considered as a full thermomechanical process, while viscoelastic and (visco)plastic deformations are dissipative and lead to self-heating. Most often, the thermal and mechanical boundary conditions are chosen in a way that the temperature evolution is negligible. If not, a suitable combination of loading regime and thermal boundary condition is exploitable for material characterization by solving a coupled thermomechanical problem [Muraccione et al. (2008); Guzmán et al. (2010); Knysh and Korkolis (2015)].

Deformation processes going beyond thermoelasticity and covering a transfer of internal energy to dissipation and finally from an internal heat supply to a temperature evolution is connected to load-induced modifications of the microstructure, which plays an important role in describing the material behaviour of an actual component in its lifetime with a complex loading history and is a major topic in engineering and material science.

In recent years, the successfully employed analytical methods, numerical simulations and measurement principles for metals and alloys have been applied to other material classes and the capability of specific material models to sub-sets of new design materials has been improved. The complex methodology w.r.t. cyclic loading of metals incorporating viscoplasticity has been widely studied (e.g. in Chaboche (1989) and many other contributions).

When a specimen on the load path is subjected to an intermediate holding period and furthermore a relaxation is observed, HAUPT assigned the term *equilibrium hysteresis* to a repeated holding period on a complete load cycle Haupt (2002). According to the associated material scheme, rate-dependency with an equilibrium hysteresis is classified as general viscoplastic behaviour. Hence, one observes a significant temperature rise due to inelastic deformation at a sufficiently high strain rate and in a subsequent holding period, the temperature drops due to a dominating heat conduction from the specimen to the environment. Therefore, the load regimes, that Haupt (2002) discussed, serve as a proof of viscoplastic behaviour.

Two different viscoplastic material models are considered in this contribution. The first model was proposed in Bodner and Lindenfeld (1995) and abstained from introducing a yield condition. The extended model of Bröcker and Matzenmiller (2013)

* E-mail address: holger.sparr@b-tu.de

as the second approach is based on a rheological network with an explicit yield condition. In a first setting the experimental findings in [Chrysochoos et al. \(1989\)](#) are confirmed by the to models and furthermore compared to the elastic-plastic approach of [Kamlah and Haupt \(1998\)](#). Secondly, an optimised parameter set from a pure mechanical modelling approach is post-evaluated thermomechanically. And finally, own experimental data based on a loading regime originally suggested in [Bodner and Partom \(1975\)](#) are evaluated and discussed.

Therefore the section 2 summarises the general thermomechanical framework and highlights the most important aspects of the material models mentioned above. The following section continues with the description of the experimental setups in the two settings referred to before. Afterwards the numerical results are presented and assessed.

2 Thermomechanical Framework and Material Models

2.1 Governing principles and equations

To account for an evolving temperature field in a thermomechanical analysis, we start with the second fundamental law of thermodynamics. Incorporating the balances of energy¹ and the balance of entropy into the second law of thermodynamics leads to the inequality for the internal dissipation δ (CLAUDIUS-DUHEM inequality) (1) with \mathbf{q} as the heat flux vector, $\boldsymbol{\sigma}$ as the CAUCHY stress tensor, $\dot{\boldsymbol{\varepsilon}}$ as strain rate tensor, \mathbf{g} as the temperature gradient and ρ as the density. The introduced symbols, which are not denominated here explicitly, are explained in following paragraphs.

$$\delta = \frac{1}{\rho} \boldsymbol{\sigma} \cdot \dot{\boldsymbol{\varepsilon}} - \dot{\psi} + \theta \dot{\eta} - \frac{1}{\rho \theta} \mathbf{q} \cdot \mathbf{g} \geq 0 \quad (1)$$

Considering small deformations the usual additive split of the strain tensor $\boldsymbol{\varepsilon}$ into an elastic ($\boldsymbol{\varepsilon}^e$), a plastic ($\boldsymbol{\varepsilon}^p$) and, also quite common, a thermal part is applied (2), where the thermal part is an isotropic volume expansion indicated by the product of the thermal expansion coefficient α , the temperature change (difference of current θ to the reference temperature θ_0) and the unity tensor \mathbf{I} . In terms of the principle of equipresence the specific free energy Ψ in (3), the specific internal energy e , the specific entropy η and the stress tensor $\boldsymbol{\sigma}$ depend on the same set of variables, while the variables denoted by \mathbf{a}_i represent internal variables and are either scalar or tensor valued. With the assumptions that the named entities depend on the difference ($\boldsymbol{\varepsilon} - \boldsymbol{\varepsilon}^p$) the list of dependencies can be altered and switched to the elastic strain tensor ([Kratohvil and Dillon \(1969\)](#)).

$$\boldsymbol{\varepsilon} = \boldsymbol{\varepsilon}^e + \boldsymbol{\varepsilon}^p + \alpha(\theta - \theta_0)\mathbf{I} \quad (2)$$

$$\Psi = \hat{\Psi}(\boldsymbol{\varepsilon}, \boldsymbol{\varepsilon}^p, \theta, \mathbf{a}_1, \dots, \mathbf{a}_n) \stackrel{!}{=} \hat{\Psi}(\boldsymbol{\varepsilon}^e, \theta, \mathbf{a}_1, \dots, \mathbf{a}_n) \quad \text{and} \quad \Psi = e - \theta \eta \quad (3)$$

$$\mathbf{g} = \nabla \theta \quad \text{and} \quad \mathbf{q} = -k \mathbf{g} \quad (4)$$

The coupling of the independent variables is completed by assuming Fourier's law (4), where the positive thermal conductivity k is the proportionality factor between the heat flux and the negative temperature gradient.

The constitutive consequences for thermodynamically admissible processes are given in eqn. (5) and (6):

$$\eta = -\frac{\partial \hat{\Psi}}{\partial \theta} \stackrel{!}{=} \alpha \frac{\partial \hat{\Psi}}{\partial \boldsymbol{\varepsilon}^e} - \frac{\partial \hat{\Psi}}{\partial \theta} \quad (5)$$

$$\boldsymbol{\sigma} = \rho \frac{\partial \hat{\Psi}}{\partial \boldsymbol{\varepsilon}^e} \quad \text{with} \quad \boldsymbol{\sigma} = p \mathbf{I} + \mathbf{S} \quad , \quad (6)$$

which leads furthermore to the CLAUDIUS-DUHEM inequality in the form:

$$\delta = \frac{1}{\rho} \boldsymbol{\sigma} \cdot \dot{\boldsymbol{\varepsilon}}^p - \sum_{j=1}^n \frac{\partial \hat{\Psi}}{\partial \mathbf{a}_j} \dot{\mathbf{a}}_j - \frac{1}{\rho \theta} \mathbf{q} \cdot \mathbf{g} \geq 0 \quad . \quad (7)$$

Assuming that the internal dissipation is completely transferred into heat, the energy balance delivers an additional equation for calculating the evolving temperature field. It should be noted, that according to for instance [Helm \(2006\)](#) and [Shutov and Ihlemann \(2011\)](#) the constitutive ansatz for the free energy might be extended to include certain parts not related to any hardening mechanisms. These phenomenological and micromechanically justified approaches introduce new material parameters to control the amount of dissipation consistently. In the next two subsections, expressions for the internal dissipation are laid down for the two distinct viscoplastic material models under consideration following the outlined ansatz for the free energy.

To discuss the thermomechanical analysis in more detail, additional energy related quantities are defined by having a closer look at the first two summands of eq. (7). The first summand is denoted as the specific *plastic stress power* e_p , while the second is often called specific *rate of stored energy of cold work* e_s :

$$e_p := \frac{1}{\rho} \boldsymbol{\sigma} \cdot \dot{\boldsymbol{\varepsilon}}^p \quad \text{and} \quad e_s := \sum_{j=1}^n \frac{\partial \hat{\Psi}}{\partial \mathbf{a}_j} \dot{\mathbf{a}}_j \quad . \quad (8)$$

¹neglecting the heat supply per unit mass

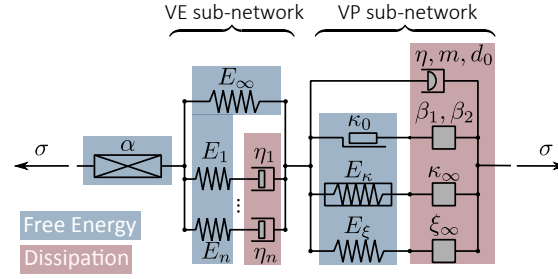


Fig. 1: Modified rheological network (originally proposed by Bröcker and Matzenmiller (2013))

The expression for the plastic work and the stored energy of cold work can then be obtained by time integration:

$$w_p = \int_{t_0}^t e_p(\tau) d\tau \quad \text{and} \quad w_s = \int_{t_0}^t e_s(\tau) d\tau \quad (9)$$

To quote Kamlah and Haupt (1998): “It is common use to plot the ratio w_s/w_p over the plastic work or the plastic strain. Besides the instantaneous rate of energy storage, [the ratio] $\varphi := e_s/e_p$ as a function of w_p is considered, since it **reflects the dynamics of dislocational processes.**” The rate of the energy storage to the plastic stress power ratio φ is also referred to as (rate of) energy transformation ratio (ETR) and gives insight into the reasonability and the physics of the considered deformation process. Identical or similar formulations can be found in Oliferuk and Raniecki (2018), Håkansson et al. (2008), Helm (2006), Johnsen et al. (2019) and others. To illustrate the calculated results the ETR (φ) is depicted in the graphs of section 4.

Since the model analysis is conducted for pure one-dimensional loading the tensor notation is dropped in the subsequent equations, which also suits the rheological network approach in the next section. For further derivation of the complete set of the differential equations we assume only small temperature changes, which means that the material parameters are temperature-independent. Furthermore the deformation process does not influence the parameters for heat conduction and heat capacity.

2.2 Rheological network with yield condition

The intuitive fundamental network rules (equal stress in consecutive network members in separated branches; equal strain in parallel branches) simplifies the generation of complex material models by connecting a set rheological elements. A network member is understood as either a single rheological element (e.g. the thermal expansion element as the first chain member from the left in Fig. 1) or a so-called sub-network (here the viscoelastic resp. viscoplastic sub-network following the thermal expansion element in the same figure).

By introducing expressions for the free energy ψ_i of each element type i and the association of the general internal variables \mathbf{a}_i to specific deformation mechanisms according to the assumed network the implementation point of experimentally motivated material models is achieved. The main idea followed by Bröcker and Matzenmiller (2013) is the classification of each element contributing purely either to free energy or to internal dissipation as indicated by the colours in Fig. 1. Therefore an original element (e.g. the traditional friction element) might be represented now by two elements to separate the energetic contributions. For the actual mathematical expression and the detailed corresponding arguments based on experimental observations for each rheological element the authors of this article would like to refer the reader to the original publication.

In the modification of the original network depicted here, the singular linear elastic spring on position two of the main chain is replaced by a viscoelastic sub-network (generalised Maxwell element) to cover viscous deformation below the elastic limit, which becomes relevant when polymer based material come into focus. The elastic limit or yield point is realised by the friction element, there the modification needs to take place outside the viscoplastic sub-network. Taking into account this modification, the internal variable belong either to the viscoelastic ($(\cdot)_{ve}$) or the viscoplastic ($(\cdot)_{vp}$) sub-network (cf. (12)).

With the aforementioned assumption that the difference $(\varepsilon - \varepsilon_{vp})$ enters the list of dependencies, the free energy for the one-dimensional case reads:

$$\varepsilon = \varepsilon_{ve} + \varepsilon_{vp} + \alpha(\theta - \theta_0) \quad (10)$$

$$\Psi = \hat{\Psi}(\varepsilon_{ve}, \theta, \mathbf{a}_1, \dots, \mathbf{a}_k, \mathbf{a}_{k+1}, \dots, \mathbf{a}_l) \quad (11)$$

Again this leads to the CLAUDIUS-DUHEM inequality in the following form for the one-dimensional case:

$$\delta = \left(\frac{1}{\varrho} \sigma - \frac{\partial \psi}{\partial \varepsilon_{ve}} \right) \dot{\varepsilon}_{ve} + \left(\frac{1}{\varrho} \sigma \alpha_{th} - \frac{\partial \psi}{\partial \theta} - \eta \right) \dot{\theta} + \frac{1}{\varrho} \sigma \dot{\varepsilon}_{vp} - \frac{\partial \psi}{\partial \mathbf{a}_{ve}} \cdot \dot{\mathbf{a}}_{ve} - \frac{\partial \psi}{\partial \mathbf{a}_{vp}} \cdot \dot{\mathbf{a}}_{vp} - \frac{1}{\varrho \theta} q \frac{\partial \theta}{\partial x} \geq 0 \quad (12)$$

where the expression \mathbf{a}_{ve} (resp. \mathbf{a}_{vp}) collects the internal variables with the index from 1 to k (resp. from $k+1$ to l) regarding the corresponding sub-network.

Therefore the n viscoelastic branches do have an impact on the true stress, the entropy and the internal dissipation as the detailed constitutive consequences (13) show.

$$\sigma = \varrho \frac{\partial \psi}{\partial \varepsilon_{ve}}; \quad \eta = \frac{1}{\varrho} \sigma \alpha_{th} - \frac{\partial \psi}{\partial \theta} = \alpha_{th} \frac{\partial \psi}{\partial \varepsilon_{ve}} - \frac{\partial \psi}{\partial \theta} \quad \text{and} \quad \frac{1}{\varrho} \sigma \dot{\varepsilon}_{vp} - \frac{\partial \psi}{\partial \mathbf{a}_{ve}} \cdot \dot{\mathbf{a}}_{ve} - \frac{\partial \psi}{\partial \mathbf{a}_{vp}} \cdot \dot{\mathbf{a}}_{vp} - \frac{1}{\varrho \theta} q \frac{\partial \theta}{\partial x} \geq 0 \quad (13)$$

The equation of heat conduction then follows from the local balance of energy. It depends on the sign of the spatial temperature gradient \mathbf{g} how the heat flux is contributing to the temperature evolution. The equation of heat conduction can be expressed as:

$$c_d \dot{\theta} = -\theta \frac{\partial \eta}{\partial \varepsilon_{ve}} \dot{\varepsilon}_{ve} - \frac{\partial(\psi + \theta \eta)}{\partial \mathbf{a}_{ve}} \cdot \dot{\mathbf{a}}_{ve} + \frac{1}{\rho} \sigma \dot{\varepsilon}_{vp} - \frac{\partial(\psi + \theta \eta)}{\partial \mathbf{a}_{vp}} \cdot \dot{\mathbf{a}}_{vp} + \frac{1}{\rho} \operatorname{div} \mathbf{q} \quad (14)$$

The first summand reflects the thermoelastic coupling and the second term corresponds to the dissipation in all MAXWELL elements of the viscoelastic sub-network. The next two terms of the sum belong to the viscoplastic sub-network. It can be seen, that the plastic stress power as the third term is not completely transferred into heat. A fraction of the mechanically introduced energy is stored as internal energy.

Eqn. (15) to (19) summarise the core of the initial value problem to solve.

$$\sigma = E^* \varepsilon_{ve} = E^* (\varepsilon - \varepsilon_{vp} - \alpha_{th} \theta) \quad \text{with } E^* = E^*(t) \quad \text{and} \quad \lim_{t \rightarrow -\infty} E^*(t) = E_\infty \quad (15)$$

$$\text{with eqns for } \dot{\varepsilon}_{\eta_i} = \dot{\varepsilon}_{\eta_i}(\dot{\varepsilon}_{ve})$$

$$\mathcal{E}_\sigma := \left\{ (\sigma, \xi, \kappa) \in \mathcal{R} \times \mathcal{R} \times \mathcal{R} \mid f(\sigma, \xi, \kappa) \leq 0 \right\} \quad \text{with } f(\sigma, \xi, \kappa) = |\sigma - \xi| - (\kappa_0 + \kappa) \quad (16)$$

$$\dot{\varepsilon}_{vp} = \frac{1}{\eta} \left\langle \frac{f}{d_0} \right\rangle^m \operatorname{sgn}(\sigma - \xi) \quad \text{with eqns for } \dot{\varepsilon}_\beta = \dot{\varepsilon}_\beta(\dot{\varepsilon}_{vp}), \quad \dot{\xi} = \dot{\xi}(\dot{\varepsilon}_{vp}) \quad \text{and} \quad \dot{\kappa} = \dot{\kappa}(\dot{\varepsilon}_{vp}) \quad (17)$$

$$\dot{\varepsilon}_{th} = \alpha_{th} \dot{\theta} \quad (18)$$

$$c_d \dot{\theta} = -\frac{1}{\rho} E \alpha_{th} \dot{\varepsilon}_{ve} + \frac{1}{\rho} \lambda \nabla \cdot (\nabla \theta) + \delta_{mat} \quad \text{with } \delta_{mat} = \frac{1}{\rho} \left[f + \delta_{\kappa_0} + \delta_\kappa + \delta_\xi \right] \dot{\varepsilon}_{vp} + \delta_{ve} \geq 0 \quad (19)$$

The first two equations cover the viscoelastic domain. The yield condition in eq. (16) incorporates kinematic and isotropic hardening, where ξ represents the backstress to shift the yield surface in stress space. Eq. (17) collects the evolutionary equations for the mechanical deformation fractions. The entity $\dot{\varepsilon}_\beta$ resembles the strain evolution in the dissipative element of the friction path in the rheological network (Fig. 1). The internal variables for hardening ξ and κ account for saturation effects (see Bröcker and Matzenmiller (2013)). The coupling is given through eq. (18) and the equation of heat conduction (19) completes the set. The full problem formulation has to be accompanied by the initial conditions, which are an undeformed stress-free state at room temperature. The initial values of the evolving inner variables are given by the (identified) material parameters (cf. sections 5.1 and 5.2).

2.3 Model without yield condition and additional constitutive assumption for free energy

The second material model investigated is based back to the very first publication Bodner and Partom (1975) and has been refined or adjusted ever since. The thermomechanical consistent material model was published in Bodner and Lindenfeld (1995) 20 years later without following the approach by Chrysochoos *et al.* described above to quantify the amount of dissipation. Instead the authors suggested well designed shear tests (decoupling strategy) to overcome the difficulties of an accurate temperature measurement.

Considering again the fundamentals outlined above, evolutionary equations for the viscoplastic strain as well as for the internal variables forming an initial value problem are the objective.

The viscoplastic strain rate is proportional to the stress deviator (20), while the factor λ is bound to a well-designed exponential function with saturation.

$$\dot{\varepsilon}^p = \lambda \mathbf{S} \quad (20)$$

$$\lambda^2 = D_2^p / J_2 \quad \text{with} \quad D_2^p = \frac{1}{2} \dot{\varepsilon}^p \cdot \dot{\varepsilon}^p \quad \text{and} \quad J_2 = \frac{1}{2} \mathbf{S} \cdot \mathbf{S} \quad (21)$$

The power function obtained the following structure:

$$D_2^p = D_2^p(J_2) = D_0^2 \exp \left[- \left(\frac{Z^2}{3J_2} \right)^n \right] \quad (22)$$

where Z represents a material state and combines all internal variables into a single scalar. The hardening approach in this form is quite unique and splits the deformation processes into isotropic and directional hardening:

$$Z = Z^I + Z^D \quad (23)$$

Both, isotropic and directional, hardening parameters are proportional to the plastic stress power. To cover well described phenomenological effects the original function for Z^I resp. Z^D has been improved and enriched.

$$\dot{Z}^I = m_1 (Z_1 - Z^I) \dot{W}_p \quad \text{with } Z^I(0) = Z_0, \quad \dot{W}_p = \mathbf{S} \cdot \dot{\varepsilon}^p \quad \text{and} \quad m_1 = m_{11} + m_{12} \exp(-m_{13} Z^I) \quad (24)$$

$$\dot{Z}^D = \beta \cdot \mathbf{U} \quad \text{and} \quad \dot{\beta} = m_2 (Z_3 \mathbf{U} - \beta) \dot{W}_p \quad \text{with } \beta(0) = \mathbf{0}, \quad \mathbf{U} = \frac{\sigma}{|\sigma|} \quad \text{and} \quad m_2 = m_{21} + m_{22} \exp(-m_{23} Z^D) \quad (25)$$

Due to the assumed small temperature changes the original terms for considering thermal recovery in (24) and (25) are neglected.

Eq. (26) serves as an additional constitutive assumption by introducing four new material parameters (a , b , p_1 and p_2).

$$\Psi_Z = \frac{a}{\varrho} \left(\frac{Z^I}{Z_1} \right)^{p_1} + \frac{b}{\varrho} \left(\frac{\boldsymbol{\beta} \cdot \boldsymbol{\beta}}{Z_3^2} \right)^{p_2} \quad (26)$$

By choosing the exponents $p_1 = 2$ and $p_2 = 1$ a quadratic form is achieved but might not reflect the desirable non-linearity. Kamlah *et al.* argued with the analogy to thermoelasticity and developed their model with a quadratic energy expression as well. In the original paper Bodner *et al.* operate with $p_1 = 4$ for copper specimen.

The expressions for the rate $\dot{\Psi}_Z$ (rate of stored energy of cold work):

$$\dot{\Psi}_Z = p_1 \frac{a}{\varrho} \frac{\dot{Z}^I}{Z_1} \left(\frac{Z^I}{Z_1} \right)^{p_1-1} + 2p_2 \frac{b}{\varrho} \frac{\boldsymbol{\beta} \cdot \dot{\boldsymbol{\beta}}}{Z_3^2} \left(\frac{\boldsymbol{\beta} \cdot \boldsymbol{\beta}}{Z_3^2} \right)^{p_2-1} \quad (27)$$

and the mechanical fraction of the internal dissipation δ_M

$$\delta_M = \frac{1}{\varrho} \dot{W}_p - p_1 \frac{a}{\varrho} \frac{\dot{Z}^I}{Z_1} \left(\frac{Z^I}{Z_1} \right)^{p_1-1} - 2p_2 \frac{b}{\varrho} \frac{\boldsymbol{\beta} \cdot \dot{\boldsymbol{\beta}}}{Z_3^2} \left(\frac{\boldsymbol{\beta} \cdot \boldsymbol{\beta}}{Z_3^2} \right)^{p_2-1} \geq 0 \quad (28)$$

are then straightforward and lead to similar structured equation of heat conduction as presented above. Having the equations outlined above at hand, a similar rheological network in analogy to the Bröcker–Matzenmiller model with just a single viscoplastic sub-network can be drawn (cf. Fig. 2). The elements in the viscoplastic sub-network represent the analytical non-linearity of the function above. A separation of internal dissipation and free energy is possible by eq. (26), while the internal variables Z^I resp. $\boldsymbol{\beta}$ appear in the dissipative element on top and the corresponding non-linear spring.

For the solution of this system of differential equations the same initial conditions apply as stated at the end of the previous section.

3 Experiments

3.1 Caloric resp. temperature measurement in tensile test for the XCrNi18.9 stainless steel

In 1998, Kamlah & Haupt presented their thermomechanical elastoplastic model by proving it against experimental data provided by the group of Chrysochoos. The XCrNi18.9 stainless steel material behaviour was investigated by tensile testing at room temperature.

Reliable experimental data depend on a sophisticated measurement strategy, which was established in two distinct ways in the group of Chrysochoos. The first method is the application of a microcalorimeter with a suitable calibration scheme.

The second method is based on measuring the temperature evolution and a calibration of the heat losses due to radiation and conduction for the plain thermoelastic effect. Convection heat losses were eliminated by a primary vacuum chamber. In contrast to the thermography applied in our own experiments the observation zone is limited to a rectangle of 15 mm × 25 mm. Current IR cameras with an increased pixel field on the detector can cover the complete sample and its surroundings (essentially the grips of the testing machine). The experiments are quantitatively evaluated by solving the heat conduction equation for the observation zone.

Both methods lead to results in close agreement, which validates the experimental findings at low strain rates of 10^{-4} 1/s.

3.2 Change of strain rate in tensile test for the copper

The setup for our own experiments is similar as outlined above but chosen to be as simple as possible, which excludes any special measures to control the thermal boundary conditions. The tests were conducted at room temperature. Flat copper samples with a thickness of 1.5 mm (standard: DIN 50125 - Shape Type H) were tested under different loading conditions. The reflection of sample surface were eliminated by blackening.

As the observing camera the ImageIR 8300 of InfraTec was applied, which is characterised by a detector format of 640 × 512 pixel, a temperature resolution of at least 0.02 K at room temperature and a usable frame rate of 100 Hz. The data evaluation is conducted interactively on the IR images by averaging the temperature values measured on well-defined geometric objects on the sample surface. The averaging reduces the thermal noise due to reflexions of the surroundings and inhomogenous emission

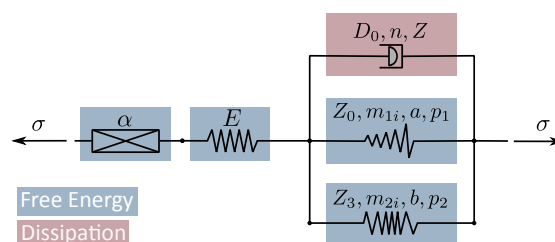


Fig. 2: Rheological analogy of the Bodner–Lindenfeld model



Fig. 3: Stress-strain curves (*left*) and temperature evolution (*right*) for a uni-axial tension (XCrNi18.9 stainless steel)



Fig. 4: Energy transformation ratio over plastic strain (*left*) resp. plastic work (*right*) for a uni-axial tension (XCrNi18.9 stainless steel)

properties on the sample surface. The thermal noise can be minimised by an additional radiation sources pointed on the sample. This heat source needs to be reflected in the heat conduction equation appropriately, which is still under investigation. Temperature profiles along and perpendicular to the loading direction are assessed as well.

The load was applied on a servohydraulic testing machine of a maximal possible load of 25 kN where the grips are not thermally decoupled to the pressure aggregates. The temperature of the upper grip is directly connected to the piston and is observably elevated compared to the lower grip. The lower grip behaves nearly as an ideal heat sink at constant temperature, while the temperature of the upper grip is slowly increasing in time of operation. Nonetheless the upper grip temperature can be assumed constant for loadings times lower than 500 s .

The applied loading scheme was adopted from the paper [Bodner and Partom \(1975\)](#). The authors suggested a displacement controlled rate change during a simple tensile test. The rate change covers approximately two orders of magnitudes. The test starts with a lower rate of $1.34 \cdot 10^{-4} 1/s$ up to a total strain value of 0.026 and increases then to $1.29 \cdot 10^{-2} 1/s$ up to a total strain value of 0.079. It follows a second lower rate load increase up to total strain value of 0.106 and a subsequent unloading at a rate $-6.80 \cdot 10^{-4} 1/s$.

The evaluation of the machine data confirmed the constant strain rates in each section of the load path. The evaluation of the experimental data for the true stress accounts for a cross-section reduction, while the numerical calculation remains in stress-strain space and therefore reflects a point-wise evaluation without considering the actual dimensions of the specimen and justifies total strain values up-to 0.1 .

4 Numerical evaluation and comparison to experimental data

4.1 Caloric evaluation of tensile test

The diagrams in Fig. 3 and 4 gather the responses of three different material models. The parameter set for the Bröcker-Matzenmiller (BM) model is chosen to reflect approximately rate-independent behaviour ($\eta = 1.0$ s). In the Bodner-Lindenfeld (BL) model the viscous deformation fraction is not clearly controllable by a single parameter, therefore its response is by model definition rate-dependent. The data of the rate-independent Kamlah-Haupt (KH) model is added as a source of a stress-strain curve to compare to and as a further reference in the remaining diagrams. The nominal (engineering) strain is used in all diagrams with the strain on the abscissa.

With an optimised parameter set both material models to be investigated are able to reflect the stress-strain curve given by the parameter set in [Kamlah and Haupt \(1998\)](#) (cf. Fig. 3 *left*). Minor deviations are visible for the BM model in the transition range of purely elastic to elastoplastic deformation.

To compare the temperature evolution artificial adiabatic boundary conditions have been formulated, since the experimental data of the temperature-time are not available. The diagram in Fig. 3 *right* shows a larger deviation of the BM model to the other two formulations of ≈ 1.7 K at the end of the load path. The thermoelastic effect in the elastic deformation range is covered by all three models.

Even more significant deviations can be found in the energy transformation ratio (ETR) plotted in Fig. 4 over the plastic (*left*) resp. over the plastic work (*right*). The KH model meets the maximum of the ETR at a plastic strain of about 0.03, but the overall qualitative behaviour is approximated better by the BL model. The quasi-rate-independent ETR-curve of the BM model has its

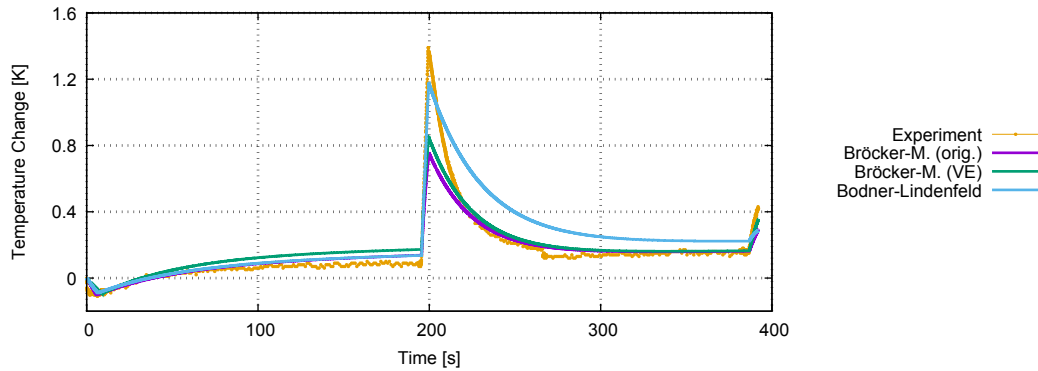


Fig. 5: Temperature evolution curves for a tensile test with two different strain rates and final unloading (flat copper specimen)

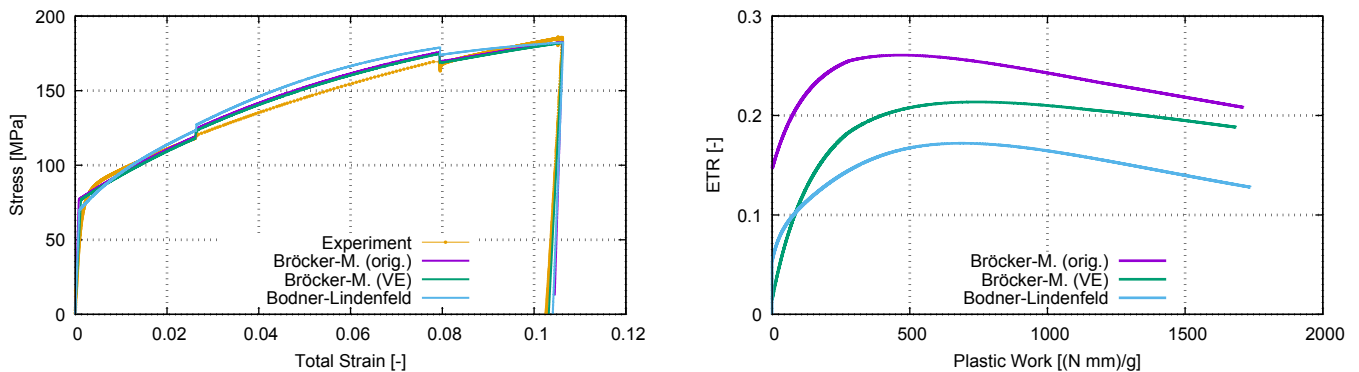


Fig. 6: Stress-strain (*left*) and ETR-plastic work (*right*) curves for a tensile test with two strain rates and final unloading (flat copper specimen)

maximum at the very beginning of the plastic deformation. Looking at the curves plotted over the plastic work, it is remarkable that the maximum value of plastic work of the KH model is almost 20% lower than the other two maxima. Therefore the absolute fraction of stored energy of cold work is lower likewise in the KH model.

4.2 Change of strain rate in tensile test

The data in the following three diagrams (Fig. 5 and 6) assemble the measured values and the calculated values of the original BM model, the extended BM model and the BL model for copper samples. The extension of the Bröcker-Matzenmiller model includes just one single Maxwell element in the viscoelastic sub-network.

In the analysis of the tensile test with alternating strain rate the adiabatic thermal boundary conditions are not valid. In Kamlah *et al.* an analytical solution was suggested, which assumes a constant temperature value for both grips. As outlined in section 3.2, the temperature evolution observed in the grips does not match the presumption of this analytical approach. Therefore the identical assumption as proposed in Chrysochoos *et al.* (1989) was chosen. It suggests an additional linear term for the rate of temperature to account for the heat losses in the equation of heat conduction (cf. eq. (19)). The corresponding additional parameter captures the ambient conditions, the specimen shape as well as the heat transfer at the grip-sample interface integratively. This parameter can be calibrated for the expected temperature range.

In Fig. 5 the different temperature-time curves for the full testing period are plotted. All curves start with a thermoelastic cooling phase at the lower strain rate. The turning pointing after ca. 10 s indicates the beginning of plastic deformation associated with internal dissipation. Until the end of the first lower strain rate section the balance of heat supply and heat loss is nearly approached. In the second section of the higher strain rate, the temperature change is strongly increasing and a maximum in the experimental data of 1.4 K is found at the end of the section at 200 s. It follows a period of temperature equalisation in the third section of the lower strain rate. The unloading is matched by a thermoelastic heating.

The optimised parameter sets for all models reflect the general behaviour, while the BL model approximates the maximum significantly better than the original and the extended BM model. It is noted here that the BM model for copper operates with an elevated module of elasticity taking the additional viscous model capability of the viscoelastic sub-network into account. This is visible in the unloading section in the left diagram of Fig. 6 where the slope is best matched by the extended BM model.

The accompanying results of the stress-strain resp. ETR-plastic work curves are shown in Fig. 6. A good agreement of experimental and model data is observed in the stress-strain curves on the *left*. It is pointed out, that the effect of the viscoelastic extension is slightly visible by a reduced slope in the (visco-)elastic unloading section. An explanation can be found in the ETR-plastic work curves on the *right*. The maximum value of plastic work of the extended BM model is significantly smaller compared to the other two models because a fraction of plastic work is shifted to the viscoelastic sub-network. In general all curves in the right diagram exhibit a similar characteristic with the maxima at a similar position on the load path. Comparing the materials themselves the ETR maxima of the copper sample are clearly smaller than the maxima of the steel sample (see Fig. 4 *right*). This holds especially

true for the BL model.

5 Conclusion

The phenomenological approach in a thermomechanical context gives an informative insight into dissipative and conservative deformation mechanisms concerned for all discussed models. The concept of internal variables relates these mechanisms to the evolution of state variables. A more detailed evaluation produces further information in terms of mechanisms attributing to stored energy of cold work (which is not shown in this paper). In general this means, that for engineering tasks where an assessment of plastic deformation is essential, the phenomenological approach is a powerful tool and the model capabilities have been shown in both testing scenarios.

Usually the coupling due to the full thermomechanical description is neglected. The problems, that arise here, are a necessary validity check of the material parameter set and the extensibility to different loading regimes. As outlined in this paper, three curves and not just a stress-strain characteristic is used for a plausibility check.

To examine a material likewise, the experimental effort is increased, since the temperature evolution needs to be observed. But as the observations of section 4.1 show, even with unrealistic thermal boundary conditions - identical with dropping the temperature measurement altogether, the thermomechanical analysis leads to sensible parameter sets with a more solid foundation, when a thermomechanically derived state variable like the energy transformation ratio (ETR) is additionally introduced into the parameter identification process. The ETR characteristic is linked to specific materials resp. material classes and can therefore be integrated in the identification process qualitatively. Thermodynamically consistent parameter bounds were notified by [Kamlah and Haupt \(1998\)](#) and derived in [Kamlah \(1994\)](#), which is an open topic for future research.

In the second experiment with alternating strain rates differing by two orders of magnitude in a tension test with unloading, an accurate agreement is harder to achieve and the model capabilities need to be questioned. The effect of the viscoelastic extension in the Bröcker-Matzenmiller model in this setup is not particularly large, but the influence on the temperature-time as well as on the ETR-plastic work characteristic is clearly visible.

As a consequence the thermomechanical analysis is to be extended in terms of the loading regime and other design materials. More complex loading regimes like cyclic loading, tension-compression loading and an alternation of different strain rates are going to be investigated. The applicability of the extended Bröcker-Matzenmiller model and the Bodner-Lindenfeld model without a yield condition to polymer material is of major interest in future research work.

Acknowledgement

The support of the BMWi and AiF Projekt GmbH is grateful acknowledged. The authors thank Fabian Göttfert (InfraTec GmbH, Dresden) for his contribution to the experimental work.

Appendix

5.1 Parameter sets related to section 4.1

Tab. 1: Parameter set for Bodner–Lindenfeld model for the XCrNi18.9 stainless steel

Thermoelasticity			Isotropic Hardening		
Modulus of Elasticity E_∞	N mm ⁻²	200 000	Z_0	MPa	220
Density ρ	kg/m ³	7 800.0	Z_1	MPa	500
Expansion Coefficient α	K ⁻¹	$1.6 \cdot 10^{-5}$	m_{11}	MPa ⁻¹	0.01
Heat Capacity c_{def}	J/(kg K)	480.0	m_{12}	MPa ⁻¹	16.7
Thermal conductivity k	W/(m K)	20.0	m_{13}	MPa ⁻¹	0.007
Scaling factor D_0	s ⁻¹	10 000	Directional Hardening		
Exponent n	[-]	3	Z_3	MPa	340
Plastic work <i>resp.</i> Free energy parameter			m_{21}	MPa ⁻¹	0.055
Factor for isotropic h. Ψ -fraction a	MJ m ⁻³	0.02	m_{22}	MPa ⁻¹	0.23
Corr. exponent p_1	[-]	4.0	m_{23}	MPa ⁻¹	0.05
Factor for directional h. Ψ -fraction b	MJ m ⁻³	1.0			
Corr. exponent p_2	[-]	14.0			

The BM model is capable to describe isotropic as well as kinematic hardening behavior. The presented experimental data are not sufficient to calibrate the backstress ξ . Therefore the hardening mechanisms are treated equally in terms of modulus and saturation for the pure tensile loading regime (cf. Tab. 2 and Tab. 4 in the next section).

Tab. 2: Parameter set for Bröcker–Matzenmiller model for the XCrNi18.9 stainless steel

Thermoelasticity			Kinematic Hardening		
Modulus of Elasticity E_∞	N mm ⁻²	200 000	Kin. Hardening Modulus E_κ	N mm ⁻²	4 000
Density ρ	kg/m ³	7 800.0	Kin. Saturation κ_∞	N mm ⁻²	155.0
Expansion Coefficient α	KI	$1.6 \cdot 10^{-5}$	Isotropic Hardening		
Heat Capacity c_{def}	J/(kg K)	480.0	Iso. Hardening Modulus E_ξ	N mm ⁻²	4 000
Thermal conductivity k	W/(m K)	20.0	Iso. Saturation ξ_∞	N mm ⁻²	155.0
Friction Element			Viscoplasticity		
Yield Stress κ_0	N mm ⁻²	273	Strain rate scaling factor η	s	1.0
Lin. Dissipation Coeff. β_1	[-]	0.4	Strain rate exponent m	[-]	1
Non-lin. Dissipation Coeff. β_2	[-]	50			

5.2 Parameter sets related to section 4.2

Tab. 3: Parameter set for Bodner–Lindenfeld model for pure copper

Thermoelasticity			Isotropic Hardening		
Modulus of Elasticity E_∞	N mm ⁻²	80 000	Z_0	MPa	100
Density ρ	kg/m ³	8 920	Z_1	MPa	120
Expansion Coefficient α	K ⁻¹	$16.5 \cdot 10^{-6}$	m_{11}	MPa ⁻¹	1.0
Heat Capacity c_{def}	J/(kg K)	385.0	m_{12}	MPa ⁻¹	2.0
Thermal conductivity k	W/(m K)	400.0	m_{13}	MPa ⁻¹	0.01
Scaling factor D_0	s ⁻¹	10 000	Directional Hardening		
Exponent n	[-]	5	Z_3	MPa	150
Plastic work <i>resp.</i> Free energy parameter			m_{21}	MPa ⁻¹	0.18
Factor for isotropic h. Ψ -fraction a	MJ m ⁻³	0.08	m_{22}	MPa ⁻¹	0.1
Corr. exponent p_1	[-]	4.0	m_{23}	MPa ⁻¹	0.1
Factor for directional h. Ψ -fraction b	MJ m ⁻³	2.2			
Corr. exponent p_2	[-]	1.0			

Tab. 4: Parameter set for Bröcker–Matzenmiller model for pure copper

Thermoelasticity			Kinematic Hardening		
Modulus of Elasticity E_∞	N mm^{-2}	100 000	Kin. Hardening Modulus E_κ	N mm^{-2}	2 000
Density ρ	kg/m^3	8 920	Kin. Saturation κ_∞	N mm^{-2}	135.0
Expansion Coefficient α	K^{-1}	$16.5 \cdot 10^{-6}$	Isotropic Hardening		
Heat Capacity c_{def}	$\text{J}/(\text{kg K})$	385.0	Iso. Hardening Modulus E_ξ	N mm^{-2}	2 000
Thermal conductivity k	$\text{W}/(\text{m K})$	400.0	Iso. Saturation ξ_∞	N mm^{-2}	135.0
Friction Element			Viscoplasticity		
Yield Stress κ_0	N mm^{-2}	75	Strain rate scaling factor η	s	700
Lin. Dissipation Coeff. β_1	[-]	0.15	Strain rate exponent m	[-]	1.0
Non-lin. Dissipation Coeff. β_2	[-]	30			

References

- S. R. Bodner and A. Lindenfeld. Constitutive modelling of the stored energy of cold work under cyclic loading. *European Journal of Mechanics - A/Solids*, 14(3):333–348, 1995.
- S. R. Bodner and Y. Partom. Constitutive Equations for Elastic-Viscoplastic Strain-Hardening Materials. *Journal of Applied Mechanics*, 42(2):385–389, 06 1975. ISSN 0021-8936. doi: [10.1115/1.3423586](https://doi.org/10.1115/1.3423586).
- C. Bröcker and A. Matzenmiller. An enhanced concept of rheological models to represent nonlinear thermoviscoplasticity and its energy storage behavior. *Continuum Mechanics and Thermodynamics*, 25(6):749–778, 2013. doi: [10.1007/s00161-012-0268-3](https://doi.org/10.1007/s00161-012-0268-3).
- J.L. Chaboche. Constitutive equations for cyclic plasticity and cyclic viscoplasticity. *International Journal of Plasticity*, 5(3):247–302, 1989. ISSN 0749-6419. doi: [10.1016/0749-6419\(89\)90015-6](https://doi.org/10.1016/0749-6419(89)90015-6).
- N. Cholewa, P. T. Summers, S. Feih, A. P. Mouritz, B. Y. Lattimer, and S. W. Case. A technique for coupled thermomechanical response measurement using infrared thermography and digital image correlation (tdic). *Experimental Mechanics*, 56(2):145–164, 2016. doi: [10.1007/s11340-015-0086-1](https://doi.org/10.1007/s11340-015-0086-1).
- A. Chrysochoos. Infrared thermography applied to the analysis of material behavior: a brief overview. *Quantitative InfraRed Thermography Journal*, 9(2):193–208, 2012. doi: [10.1080/17686733.2012.746069](https://doi.org/10.1080/17686733.2012.746069).
- A. Chrysochoos, O. Maisonneuve, G. Martin, H. Caumon, and J.C. Chezeaux. Plastic and dissipated work and stored energy. *Nuclear Engineering and Design*, 114(3):323–333, 1989. doi: [10.1016/0029-5493\(89\)90110-6](https://doi.org/10.1016/0029-5493(89)90110-6).
- B. D. Coleman and M. E. Gurtin. Thermodynamics with internal state variables. *The Journal of Chemical Physics*, 47(2):597–613, 1967. doi: [10.1063/1.1711937](https://doi.org/10.1063/1.1711937).
- A. Yu. Fedorova, M. V. Bannikov, A. I. Terekhina, and O. A. Plekhov. Heat dissipation energy under fatigue based on infrared data processing. *Quantitative InfraRed Thermography Journal*, 11(1):2–9, 2014. doi: [10.1080/17686733.2013.852416](https://doi.org/10.1080/17686733.2013.852416).
- R. Guzmán, J. Meléndez, J. Zahr, and J. L. Pérez-Castellanos. Determination of the constitutive relation parameters of a metallic material by measurement of temperature increment in compressive dynamic tests. *Experimental Mechanics*, 50(3):389–397, 2010. doi: [10.1007/s11340-009-9223-z](https://doi.org/10.1007/s11340-009-9223-z).
- P. Haupt. *Continuum Mechanics and Theory of Materials*. Springer-Verlag, 2nd edition, 2002. doi: [10.1007/978-3-662-04775-0](https://doi.org/10.1007/978-3-662-04775-0).
- D. Helm. Stress computation in finite thermoviscoplasticity. *International Journal of Plasticity*, 22(9):1699–1727, 2006. doi: [10.1016/j.ijplas.2006.02.007](https://doi.org/10.1016/j.ijplas.2006.02.007).
- P. Håkansson, M. Wallin, and M. Ristinmaa. Prediction of stored energy in polycrystalline materials during cyclic loading. *International Journal of Solids and Structures*, 45(6):1570–1586, 2008. doi: [10.1016/j.ijsolstr.2007.10.009](https://doi.org/10.1016/j.ijsolstr.2007.10.009).
- J. Johnsen, A. H. Clausen, F. Grytten, A. Benallal, and O. S. Hopperstad. A thermo-elasto-viscoplastic constitutive model for polymers. *Journal of the Mechanics and Physics of Solids*, 124:681–701, 2019. doi: [10.1016/j.jmps.2018.11.018](https://doi.org/10.1016/j.jmps.2018.11.018).
- M. Kamlah. *Zur Modellierung des Verfestigungsverhaltens von Materialien mit statischer Hysterese im Rahmen der phänomenologischen Thermomechanik*. PhD thesis, Universität Gesamthochschule Kassel, 1994.
- M. Kamlah and P. Haupt. On the macroscopic description of stored energy and self heating during plastic deformation. *International Journal of Plasticity*, 13(10):893–911, 1998. doi: [10.1016/S0749-6419\(97\)00063-6](https://doi.org/10.1016/S0749-6419(97)00063-6).
- P. Knysh and Y. P. Korkolis. Determination of the fraction of plastic work converted into heat in metals. *Mechanics of Materials*, 86:71–80, 2015. doi: [10.1016/j.mechmat.2015.03.006](https://doi.org/10.1016/j.mechmat.2015.03.006).
- J. Kratochvil and O. W. Dillon. Thermodynamics of elastic-plastic materials as a theory with internal state variables. *Journal of Applied Physics*, 40(8):3207–3218, 1969. doi: [10.1063/1.1658167](https://doi.org/10.1063/1.1658167).
- J.-M. Muracciole, B. Wattrisse, and A. Chrysochoos. Energy balance of a semicrystalline polymer during local plastic deformation. *Strain*, 44(6):468–474, 2008. doi: [10.1111/j.1475-1305.2007.00412.x](https://doi.org/10.1111/j.1475-1305.2007.00412.x).
- P. P. Oldyrev. Self-heating and failure of plastics under cyclic loading. *Polymer Mechanics*, 3(3):322–328, 1967. doi: [10.1007/BF00858775](https://doi.org/10.1007/BF00858775).
- P. P. Oldyrev and V. P. Tamuzh. Energy dissipation in a glass-reinforced plastic during prolonged cyclic deformation. *Strength of Materials*, 1(3):244–248, 1969. doi: [10.1007/BF01543209](https://doi.org/10.1007/BF01543209).

- W. Oliferuk and B. Raniecki. Thermodynamic description of the plastic work partition into stored energy and heat during deformation of polycrystalline materials. *European Journal of Mechanics - A/Solids*, 71:326 – 334, 2018. doi: [10.1016/j.euromechsol.2018.04.002](https://doi.org/10.1016/j.euromechsol.2018.04.002).
- A. V. Shutov and J. Ihlemann. On the simulation of plastic forming under consideration of thermal effects. *Materialwissenschaft und Werkstofftechnik*, 42(7):632–638, 2011. doi: [10.1002/mawe.201100821](https://doi.org/10.1002/mawe.201100821).
- W. Thomson. XV.— On the dynamical theory of heat, with numerical results deduced from mr joule’s equivalent of a thermal unit, and m. regnault’s observations on steam. *Transactions of the Royal Society of Edinburgh*, 20(2):261–288, 1853. doi: [10.1017/S0080456800033172](https://doi.org/10.1017/S0080456800033172).
- C. Truesdell and W. Noll. *The Non-Linear Field Theories of Mechanics*. Springer-Verlag, Berlin, 3rd edition, 2004. doi: [10.1007/978-3-662-10388-3](https://doi.org/10.1007/978-3-662-10388-3).
- T. Ummenhofer and J. Medgenberg. Numerical modelling of thermoelasticity and plasticity in fatigue-loaded low carbon steels. *Quantitative InfraRed Thermography Journal*, 3(1):71–91, 2006. doi: [10.3166/qirt.3.71-91](https://doi.org/10.3166/qirt.3.71-91).